Wave Mode Discrimination of Coded Ultrasonic Guided Waves Using Two-Dimensional Compressed Pulse Analysis

Sergio Malo, Sina Fateri, Makis Livadas, Cristinel Mares, and Tat-Hean Gan

***Abstract*— Ultrasonic guided waves testing is a technique successfully used in many industrial scenarios worldwide. For many complex applications, the dispersive nature and multimode behavior of the technique still poses a challenge for correct defect detection capabilities. In order to improve the performance of the guided waves, a 2-D compressed pulse analysis is presented in this paper. This novel technique combines the use of pulse compression and dispersion compensation in order to improve the signal-to-noise ratio (SNR) and temporal-spatial resolution of the signals. The ability of the technique to discriminate different wave modes is also highlighted. In addition, an iterative algorithm is developed to identify the wave modes of interest using adaptive peak detection to enable automatic wave mode discrimination. The employed algorithm is developed in order to pave the way for further in situ applications. The performance of Barker-coded and chirp waveforms is studied in a multimodal scenario where longitudinal and flexural wave packets are superposed. The technique is tested in both synthetic and experimental conditions. The enhancements in SNR and temporal resolution are quantified as well as their ability to accurately calculate the propagation distance for different wave modes.**

***Index Terms*— Barker-coded, dispersion compensation, pulse compression (PuC), 2-D compressed analysis, wave mode discrimination.**

I. Introduction

CURRENTLY, many industries require new nondestructive testing (NDT) and structural health monitoring (SHM) solutions to provide information about the integrity status of different structures. Ultrasonic guided wave (UGW) is a worldwide NDT and SHM technique, successfully employed in many different applications on a wide range of structures [1]. Its ability to cover long distances with relatively low attenuation gives it highly promising features for many prospective new applications. However, its multimode behavior and dispersive nature can affect the signal's integrity, making its analysis a challenging task. The propagation of UGW commonly involves a multimode scenario; multiple modes are normally excited and/or originated by mode conversion. Some of these wave modes at certain frequencies can be highly dispersive. As a result of dispersion, wave packets spread over time and space, which can affect the signal-to-noise ratio (SNR), inspection resolution, and complicate signal interpretation [2]. For this reason, dispersive regions of the dispersion curves are commonly avoided for certain applications such as pipe or rod inspections. Therefore, wave mode selection and the frequency range employed could be confined to nondispersive areas. In order to overcome these challenges and improve the capabilities of the UGW technique, several investigations are currently being carried out regarding the transducer, electronic technology development, and digital signal processing (DSP) methods.

Different DSP approaches have been used in order to mitigate or remove the effect of the dispersive nature of the guided waves [2]–[5]. Wilcox *et al.* [2] proposed a signal processing technique that simulated the linear effect of dispersion as the waves propagated through the waveguide. In a later investigation, they developed a dispersion compensation technique that made use of *a priori* information about the dispersion of the wave mode to compensate the wave packet [3]. De Marchi *et al.* [5] proposed a different approach for the compensation of the waves by using the warped frequency transform (WFT) that produced a flexible sampling of the time-frequency domain. The technique was successfully tested on an aluminum irregular waveguide with different cross sections. However, these dispersion compensation techniques were not evaluated in a multimodal scenario.

As previously mentioned, the multimodal behavior of the UGW complicates the analysis of the signals; for this reason, different approaches have been used to achieve wave mode discrimination [6]–[8]. Among them, some have used the dispersion of the waves not only to restore the shape of the waves and remove the effect of the dispersion, but also to improve wave mode discrimination capabilities. Xu *et al.* [8] utilized the dispersion of the different wave modes to develop a method for wave mode separation. Dispersion compensation was applied to compress the signals and remove any overlap between the modes. Then, rectangular time windows were used to separate each mode. Mode separation was achieved and the technique was proven as a thickness estimation method. However, this method required *a priori* knowledge of distance propagation, in order to estimate the plate thickness. Following this paper, Xu *et al.* [9] proposed a wideband dispersion reversal (WDR) technique for pure wave mode compensation. Naturally dispersive target modes were selectively excited and

Manuscript received January 6, 2017; accepted April 7, 2017. Date of publication May 11, 2017; date of current version July 1, 2017. *(Corresponding author: Sergio Malo.)*

S. Malo, M. Livadas, and T.-H. Gan are with the Brunel Innovation Centre, Brunel University, Uxbridge UB8 3PH, U.K. (e-mail: tat-hean.gan@brunel.ac.uk).

S. Fateri is with Plant Integrity Ltd., Cambridge CB21 6AL, U.K.

C. Mares is with Brunel University, Uxbridge UB8 3PH, U.K.

Digital Object Identifier 10.1109/TUFFC.2017.2693319

short pulses were obtained with the use of WDR. However, the technique requires the target mode to be highly dispersive for correct implementation, which could represent a limitation in its application.

The main limitation of these techniques is that, even if the full dispersion is removed, the inspection resolution relies on the length of the excitation waveform. A Hann-windowed tone burst is commonly employed where the resolution relies on the selected number of cycles. In contrast, some authors have studied alternative excitation waveforms by using pulse compression (PuC) as a postprocessing technique. Different approaches of the PuC technique have been used in the field with promising results regarding SNR enhancements. Gan *et al.* [10], [11] employed PuC technique using a Hanning chirp signal as the excitation waveform. Garcia-Rodriguez *et al.* [12] studied the application of Golay codes by comparing the most suitable excitation bit length and the frequency response of the transducers. Recently, Zhou *et al.* [13] studied the use of PuC in combination with wavelet filtering as a hybrid method applied to air-coupled ultrasonic testing. Using a Barker code waveform as excitation, a Wavelet transform thresholding was applied previously to the matched filter. However, these previous investigations were carried out under nondispersive scenarios, where the effect of the dispersion on the performance of the PuC technique was not considered.

Due to the effect of the dispersion on the wave shape, especially for broadband excitations such as chirp waveforms, a combination of dispersion compensation and PuC techniques has been employed. Luo *et al.* [14] used Golay code PuC in combination with dispersion compensation in order to improve the inspection resolution but also to carry out mode purification. However, the SNR and resolution enhancements were not quantified as well as time of arrival (ToA) accuracy. Lin *et al.* [15] studied different PuC excitation waveforms in combination with a dispersion compensation method. The frequency content of the different waveforms was studied and adapted to the excitability of the transducer. The differences between the performances of the coded signals were studied by comparing their main lobe width (MLW) and sidelobe level (SLL). However, this analysis was done in an ideal situation with no superposition between different wave modes. No information about the accuracy of the method detecting ToA of the different wave packet was produced. Yucel *et al.* [16], [17] integrated both the aforementioned techniques in a brute-force search algorithm, and then compared the performance of maximal length sequence (MLS) and chirp excitation waveforms in terms of ToA accuracy and SNR enhancement. Their results proved the ability of the method to detect accurate ToA for flexural wave modes in multimodal and superposed scenarios. In contrast, significant errors were found experimentally for the case of longitudinal wave modes. The ability of the algorithm for accurate ToA relies on the dispersive nature of the wave mode of interest, which limits the method's application. In addition, this algorithm extracts the accurate ToA using a brute-force search method, where a suitable distance range needs to be predefined.

In this paper, PuC and dispersion compensation techniques are combined to perform wave mode discrimination and enhance the SNR and the temporal-spatial resolution of the signals. Barker-coded and chirp excitation waveforms are proposed as an alternative to the conventional tone burst waveforms. The effect of different dispersion compensations (in terms of distance) on the cross correlation response of the wave modes of concern is analyzed in two dimensions of time and distance. The 2-D compressed analysis presented allows the effects of the dispersion compensation on the cross-correlated signals to be studied, not only on the wave mode of concern, as in previous studies, but also on the other echoes present in the signals that correspond to any other wave modes. This information was used to design a novel adaptive peak detection (APD) algorithm for wave mode identification in a multimodal scenario. This iterative algorithm is mathematically efficient and allows the extraction of the wave packets present in the signal with accurate ToA and high resolution, as well as to which mode they correspond. This is done without a predefined distance range on a superposed scenario.

This paper is organized as follows. The fundamentals of the techniques are presented in Section II. The performance of the methodology on synthetic signals is presented in Section III, together with the iterative algorithm performance on the previously simulated signals. The experimental results, in order to validate the method, are included in Section IV. Finally, Section V includes the discussion and conclusions of this paper.

II. Background Theory and Proposed Methods

A. Pulse Compression

PuC is a postprocessing method that has been employed in many different applications such as radar [18] or diagnostic ultrasound [19], with the aim of increasing the excitation power introduced by the waveform while keeping the temporal-spatial resolution constant. For UGW testing applications, PuC and the use of coded excitation waveforms represent an alternative to the common use of windowed tone burst where the temporal-spatial resolution relies on the number of cycles employed. The autocorrelation properties of these coded waveforms are used to compress the signals and improve the inspection resolution. Therefore, an excitation signal with good autocorrelation properties is required. Different waveforms have been previously employed such as chirp [11], MLS [17], Golay codes [12], or Barker codes [13], [15]. The achieved resolution is dependent on the autocorrelation properties of the specific waveform employed. The received signal is cross correlated using the excitation waveform, denoted as the reference signal. The outcome of this process will generate specific peaks for those matches between the reference and the received signal. For this reason, the technique's resolution relies mainly on the cross correlation properties of the excitation waveform and not on the length of the signals. Consequently, the energy introduced into the waveguide can be increased without compromising the high-resolution of the technique if required [20]. Two alternatives to the conventional Hann-windowed excitation are

evaluated: Barker code and chirp excitations. Both waveforms have been selected due to their post-processing simplicity and the reported results of using these waveforms for UGW applications [13], [15], [17]. To determine the autocorrelation properties of the waveforms and the benefits of their use, two factors are compared: the difference between the main and side lobes of the autocorrelation function or the SLL and the MLW.

1) Barker Code : Barker codes are a series of biphase code sequences of different lengths with high autocorrelation properties. With lengths from 2 to 13 bit, most authors have focused on 11 and 13 bit lengths due to better autocorrelation properties (Table I). Barker code SLL is defined by (1) where M is the length of the sequence

$$\mathrm{SLL} = 20\log(1/M). \tag{1}$$

Barker code sequences, instead of being transmitted directly, are modulated to a base pulse sequence to adapt the signal to the transducer's frequency response [21]. A sinusoidal pulse of 50-kHz cycle was used in this paper (Fig. 1). The phase change corresponds to a change from 0° to 180° [13], [15]. Fig. 1 shows the autocorrelation properties and the frequency content of six different Barker code excitation waveforms, where the number of cycles per code bit varies from 1 to 3 for two Barker code sequence lengths: 11 and 13 bit. SLL and MLW were measured and are included in Table I. In order to measure the MLW, a threshold was applied at a level of 0.3 as was done in [15] [Fig. 1(a) and (c)].

2) Chirp: Chirped sinusoids are frequency modulated signals with a broadband bandwidth. Their wide frequency spectrum has been used as a means of studying the wave propagation properties of the waveguide. The frequency modulation of chirp signals provides them with good autocorrelation properties, optimal for application in PuC technique [15], [17], [22]. This paper employs linear chirped sinusoids, defined by

$$x(t) = \sin\left(O_0 + 2\pi\left[f_0 + \frac{f_1 - f_0}{t_1} * \frac{t}{2}\right]t\right) \tag{2}$$

where O_0 represents the initial phase, f_0 and f_1 are the starting and final frequencies, respectively, where t represents the time instances and t_1 represents the time instance at which f_1 is generated. In order to adapt the frequency response of the transducer to the frequency bandwidth of the chirp excitation signal, the following chirp was used: f_0 and f_1 are equal to 20 and 125 kHz, and $t_1 = 2$ ms (Table II). This waveform is represented in Fig. 2(a) while Fig. 2(b) and (c) shows its autocorrelation function and the frequency content of the signal. SLL and MLW are also included in Table II.

TABLE I
BARKER CODE SEQUENCE PARAMETERS

Code length (M)	Code elements	SLL (dB)	MLW (μs) for 1,2 and 3 cycles per bit
11	+++---+--+-	20.8	28, 58, 86
13	+++++--++-+-+	22.3	28, 58, 86

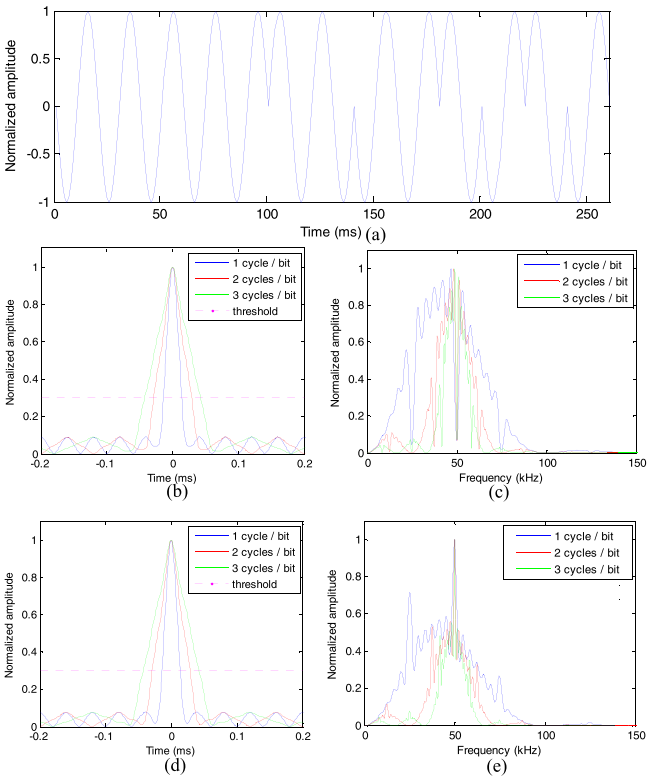

Fig. 1. (a) Barker code waveform for $M = 13$. (b) Autocorrelation functions of Barker code signals for $M = 11$. (c) Frequency content for $M = 11$. (d) Autocorrelation functions of Barker code signals for $M = 13$. (e) Frequency content for $M = 13$.

B. Dispersion Compensation

The propagation of waves, which correspond to dispersive wave modes, causes the wave packet to spread over time and space, affecting the amplitude and inspection resolution values of the signals [2]. Therefore, in the case of PuC, the postprocessing matched filter between the received signal and the reference waveform is affected by any change in the shape of the signals. The dispersion of the signals affects the applicability of the PuC technique for dispersive scenarios; this effect will be studied in Sections III and IV. Dispersion compensation was originally implemented in [3] and later applied in combination with the PuC technique in [17]. The received signal $g_d(t)$ corresponding to the propagation of a single wave mode for a specific propagation distance d can be defined as

$$g_d(t) = \int_{-\infty}^{+\infty} A(\omega)F(\omega)e^{i(-k(\omega)d+\omega t)}d\omega \tag{3}$$

where $A(\omega)$ is the reflection coefficient, $F(\omega)$ is the Fourier transform of the excited signal $f(t)$ at $d = 0$ for an angular frequency of ω. The wavenumber $k(\omega) = \omega/V_{\mathrm{ph}}$, where V_{ph} is the phase velocity. In order to eliminate the effect of the dispersion over a specific distance (d), the following expression can be used:

$$h_d(t) = \int_{-\infty}^{+\infty} G_d(\omega)e^{i(k(\omega)d+\omega(t-\tau))}d\omega \tag{4}$$

TABLE II
CHIRP WAVEFORM PARAMETERS

Length(ms)	Frequency range (kHz)	SLL (dB)	MLW (μs)
5	[20-125]	20.8	14

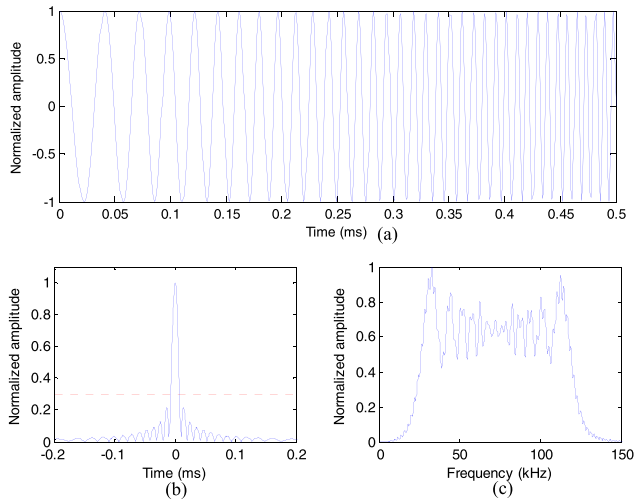

Fig. 2. (a) Linear chirp waveform. (b) Chirp autocorrelation function. (c) Frequency content.

where $G(\omega)$ is the FFT of the received signal; τ refers to the time compensation value $\tau = d/V_{\text{gr}}$ where V_{gr} is the group velocity calculated for the center frequency (f_c) of the input signal. The selection of the center frequency, which in some cases is trivial, such as Hann-windowed tone burst waveforms, could be a source of error for wideband excitation signals like chirp waveforms [3].

C. Proposed Technique and Implementation

The traditional approach for the implementation of PuC and dispersion compensation methods is illustrated in Fig. 3. It consists first of the dispersion compensation of the received signal previous to the cross correlation with the reference signal. With this technique, the specific propagation distance traveled by the wave packet is necessary. Yucel *et al.* [16] implemented this as part of an exhaustive search algorithm that compensated the signals for a range of propagation distance values before the application of the cross correlation. Once the signals were compensated for a specific distance and cross correlated, the peak value of the signal was acquired. The two principal limitations of this approach are that first, this approach requires a predefined distance range for dispersion compensation. Second, the wave packet corresponding to the specific wave mode of interest is studied separately after manual extraction from the received signal, therefore manual intervention is required.

This paper presents an alternative iterative algorithm where the specific wave mode of interest with its propagated distance does not necessarily need to be predefined. Fig. 4 shows the block diagram corresponding to the APD algorithm. The principal difference of this algorithm relies on the fact that an

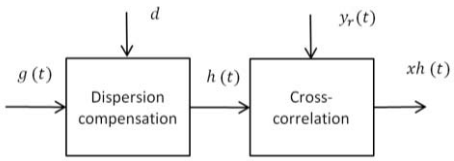

Fig. 3. Block diagram for conventional dispersion compensation and PuC implementation.

initial cross correlation between the received signal and the reference is carried out before any dispersion compensation as presented in Fig. 4(a). This is done in order to identify the candidate wave packets in the signal. Then each of these candidate wave packets is independently and separately processed. The distance compensation values, necessary to apply the dispersion compensation, are obtained by applying a peak detection (PD) algorithm [Fig. 4(a) PD1]. The minimum time increment between each candidate point is predefined as

$$t_{\min} = \text{MLW} + \delta \tag{5}$$

where δ corresponds to a small margin that was set to be 10% of the MLW. $t_{\min}$ therefore represents the minimum resolvable distance between a pair of signals. The proposed algorithm's principal advantage is that it compares the effects of the dispersion compensation in the cross-correlated results as an iteration condition as presented in Fig. 4(b). Ideally, the correct dispersion compensation fully restores the shape of the signals to that of the original input signal. Therefore, it improves the posterior cross correlation results between the received signal and the reference signal. In the same manner, the application of the incorrect dispersion compensation has the opposite effect on the waves, producing the distortion of the signals and therefore affecting the cross correlation outcome. This incorrect dispersion could be due to either over- or undercompensation of the signal. The use of the dispersion curves corresponding to a different wave mode other than the one originally propagated also has the same effect on the waves [14]. Both scenarios are used by the proposed APD algorithm to analyze first if the correct wave mode dispersion curves are being used ($dh_a > dg_i$, Fig. 4) and second, whether the result could be improved for a more accurate ToA calculation ($dh_b > dh_a$, Fig. 4). These conditions rely on the fact that if the correct wave mode dispersion compensation is applied, the match between the reference signal and the received echo is improved and, as a consequence, the amplitude of the cross correlation response is increased. Therefore, if the accuracy of distance value for the compensation is improved, the amplitude is further increased. These iterations continue until no further improvement is obtained. The robustness of the proposed algorithm will be studied in the following sections in the context of synthetic analysis and experimental results.

III. SYNTHETIC ANALYSIS

The performance of the combined PuC and dispersion compensation techniques is studied in single and multimodal

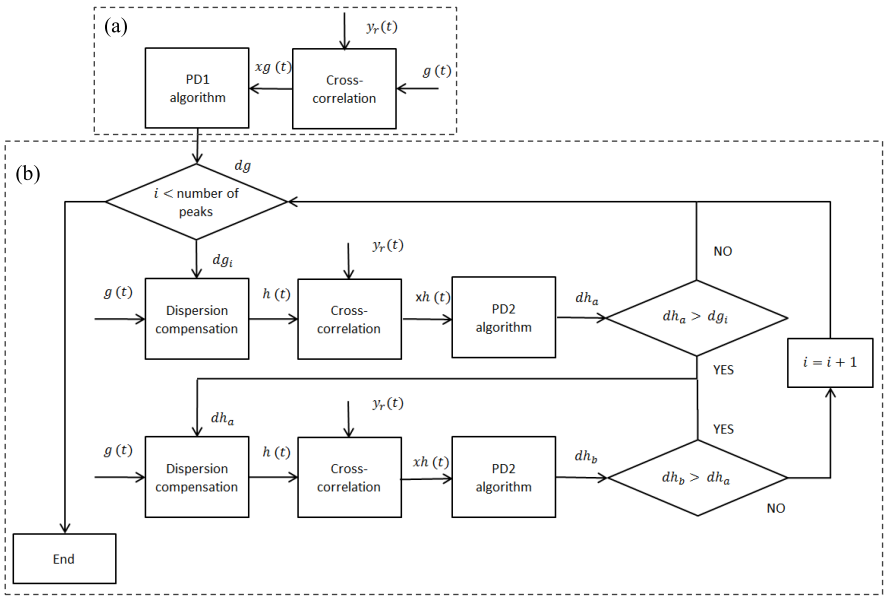

- PD1: Selects the candidate points from the cross-correlation result; a threshold is set as well as the minimum time range between points (5); returns dg with the ToA of each point.
- PD2: Finds the peak of the cross-correlation response in the time range of the previous evaluated point (dg_i).

Fig. 4. APD algorithm's block diagram for dispersion compensation and PuC iterative implementation. a) Candidate points selection. b) PuC iterative implementation.

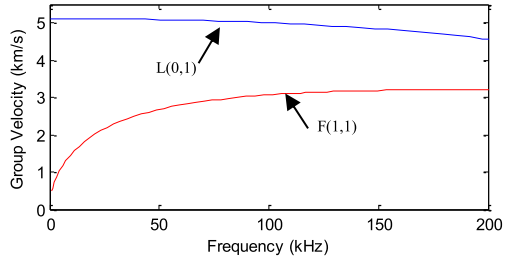

Fig. 5. Dispersion curves (group velocity) diagram for 8-mm aluminum rod including F(1,1) and L(0,1) modes.

scenarios. The waves were numerically simulated using MATLAB. In order to illustrate the advantage of the proposed technique with respect to the classic use of windowed signals, a 10-cycle Hann-windowed tone burst is also included in this analysis.

Two of the most common excitation waveforms for PuC were employed, Barker code and chirp. A Barker code signal with a single cycle per bit and a length of 13 bit was used due to its superior cross correlation properties (Table I). The chirp waveform employed was presented in Section II (Fig. 2). The simulated signals correspond to the received signal in an aluminum rod of a length of 2.15 m with pulse echo configuration, similar to that used in [16]. The dispersion curves, Fig. 5, were obtained with the use of Disperse. The analysis focused on the first 2 ms of the signal where three wave packets are present, L(0,1) first and second echoes and F(1,1) first echo. The length of the rod was decided in order to generate superposition between F(1,1) and L(0,1).

Fig. 6 corresponds to the cross correlation results after dispersion compensation using the conventional compression method (Fig. 3) for the three excitation waveforms. The red signals refer to the cross-correlated results after dispersion compensation for the second L(0,1) echo ($d = 2.15 \times 4\ m$); for the green case the dispersion compensation was performed for the first echo of F(1,1) ($d = 2.15 \times 2\ m$). The SNR, resolution, and localization accuracies obtained by both Barker code and chirp excitation waveforms were compared in Table III. The SNR, expressed in decibels, compares the peak value of the target zone and the standard deviation of the signal in the proximity of the analyzed echo [17], the resolution is defined by the MLW value of the specific wave packet [15], and the ToA error estimates the difference between the obtained ToA with the theoretical value. Chirp waveforms proved to give better resolution compared to Barker code results as expected according to their MLW. However, the SNR of both results were relatively similar. As can be observed in Fig. 6(a), Hann-windowed provided better SNR than the other two waveforms but lower resolution for both longitudinal and flexural wave modes. More importantly, Fig. 6(a) also shows how Hann-window failed to discriminate the wave modes of concern, for this reason it was excluded from the analysis of Table III. In contrast, Fig. 6(b) and (c) illustrates how the technique is able to restore highly dispersive waveforms of Barker code and chirp, respectively (first F(1,1) echo), and at the same time minimize the presence of other wave modes (longitudinal), due to the dispersion overcompensation.

In order to illustrate the effect of the compensation on the dispersive waves as well as on the nondispersive ones, a 2-D compressed analysis was designed. This analysis presents the effect of different dispersion compensations (in terms of distance) on the cross correlation response of the wave modes of concern in two dimensions of time and distance. In these 2-D compressed diagrams, the x-axis represents the time domain (ms); the y-axis corresponds to the compensated distance values (m); and the colored bar represents the normalized amplitude of the cross-correlated response. Fig. 7(a) and (b) shows the Barker code and chirp simulation results for a range of distance compensation values of [0–10 m] with an incremental resolution of 0.1 m for F(1,1) wave mode. Both cases, Barker code and chirp,

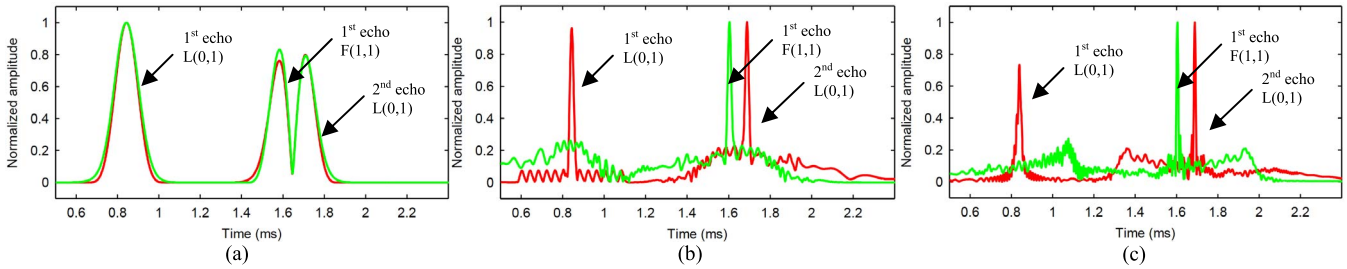

Fig. 6. (a) Simulated results for Hann-windowed, (b) Barker code, and (c) chirp excitation waveforms. Red and green lines represent the cross-correlated signal after dispersion compensation for L(0,1) and F(1,1) wave modes.

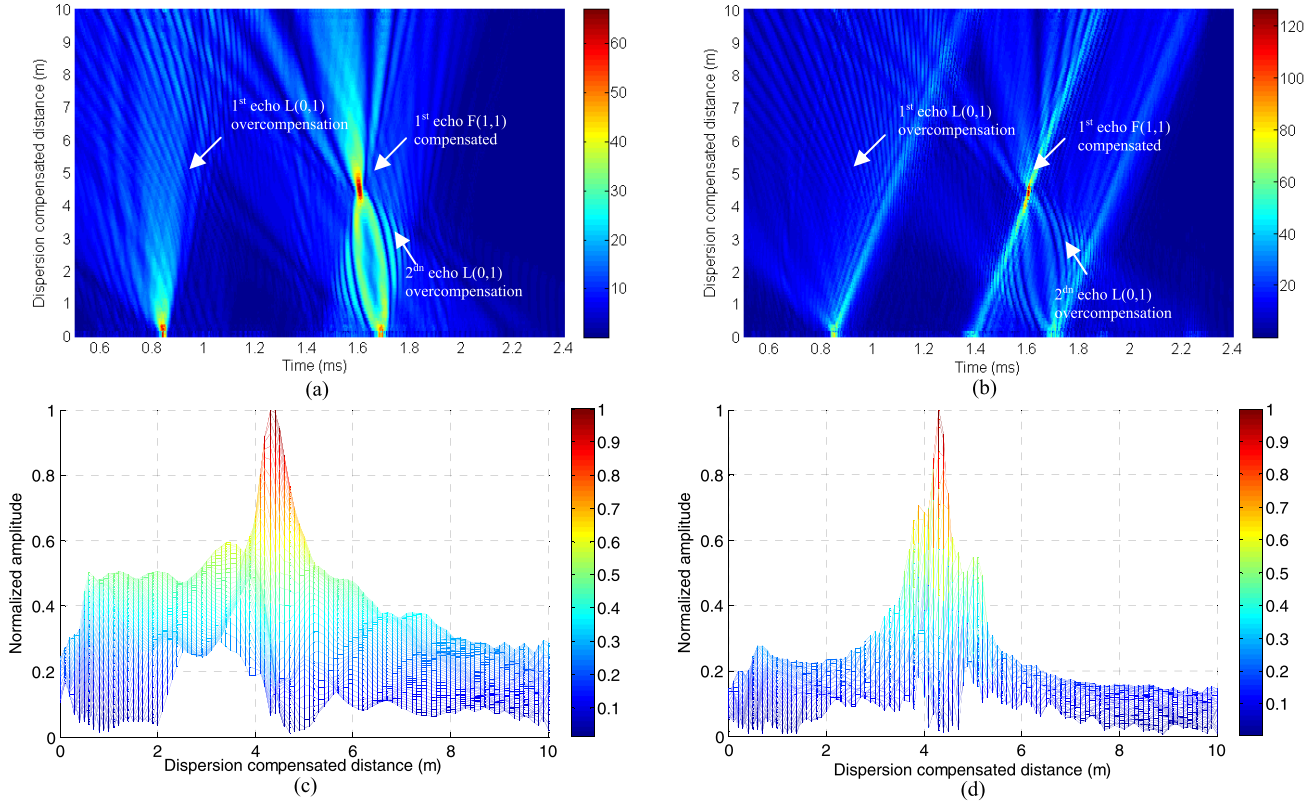

Fig. 7. Two-dimensional compressed diagram of the synthetic results for F(1,1) dispersion compensation for (a) Barker code and (b) chirp excitation waveforms, for a dispersion compensated distance range of [0–10 m]. Dispersion compensated distances axis representation of the previous 2-D compressed diagrams focused on the time range of the reconstruction of F(1,1) echo for (c) Barker code and (d) chirp excitation waveforms.

TABLE III
SIMULATED RESULTS

Waveform	Wave mode	SNR (dB)	Resolution (μs)	ToA error (%)
Barker code	L(0,1)	19.62	30	2.39
	F(1,1)	19.61	30	0.04
Chirp	L(0,1)	21.75	13	2.39
	F(1,1)	23.49	13	0.04

illustrate how the correct compensation of the dispersive wave mode was able to restore F(1,1) wave packet. This verifies the results of the analysis shown in Fig. 6(b) and (c). In addition, Fig. 7(a) and (b) shows the effect of the L(0,1) overcompensation.

Both L(0,1) echoes were detected on the initial cross correlation response without applying dispersion compensation due to low dispersion characteristics (Fig. 5). While the dispersion compensated distance value of F(1,1) increased, both echoes were overcompensated, which affected their shape and therefore reduced the cross correlation response amplitude of both echoes.

The 2-D compressed diagrams, which show the changes in the cross correlation results after dispersion compensation, can be used for accurate ToA calculation. As was presented by [17] the iterative dispersion compensation for a distance range can be used as a ToA quantification technique for flexural case. To illustrate this, the F(1,1) restored echo, previously shown in Fig. 6, is now shown in Fig. 7(c) and (d) for dispersion compensated distance axis. However, in this research no attention was given to the time domain axis. As shown in Fig. 7(a) and (b), and in Table III, this axis also provides accurate information about the specific ToA of

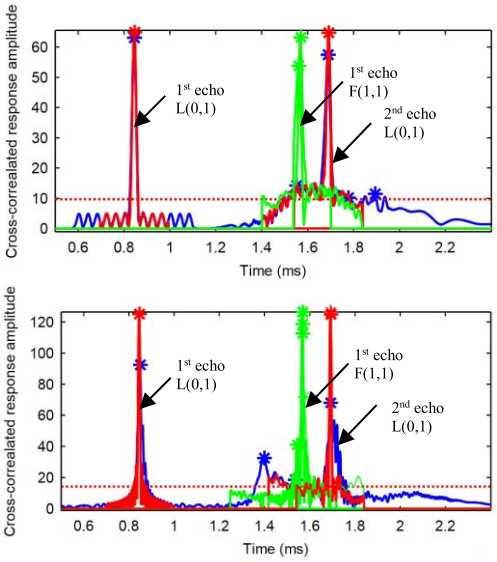

Fig. 8. Iterations' representation of algorithm result for the Barker code (top) and chirp (bottom) excitation. Blue lines: first cross correlation result. Green lines: flexural compensated iterative results after cross correlation. Red lines: longitudinal compensated iterative results after cross correlation.

the restored waveforms. In conclusion, these 2-D compressed diagrams allow for the extraction of accurate propagation distances for each wave mode. The proposed iterative algorithm combines the information of both axes, extracting the specific propagation distance from the time domain and applying the corresponding dispersion compensation accordingly. The performance of this algorithm for the simulated data is presented in Section III-A.

A. APD Algorithm Performance Analysis

The APD algorithm is tested on the simulated signals in order to illustrate its performance. The outcome of its iterative process is shown in Fig. 8 top and bottom, for Barker code and chirp excitation waveforms, respectively. The result of the initial cross correlation is represented in blue. Then, the signal response goes through a PD stage in order to identify the possible echoes of interest.

To avoid the dispersion compensation of unwanted points such as side lobes or coherent noise of the cross correlation response, a threshold is set. This threshold was selected as the double of the SLL as defined in (1). Next, the peak values of the signal above the threshold are treated as candidate echoes of the signal (blue points). If a smaller value of the threshold is selected, the number of points of study increases but no changes are expected in the results. However, the selected threshold level skips unnecessary items being fed into the dispersion compensation stage. After this, for each considered point, dispersion compensation is applied separately for each specific ToA estimate. The results of the iterative dispersion compensation for each particular wave mode compensation are represented in green and red for F(1,1) and L(0,1), respectively. For clarification, only the iterations that increase the amplitude of the wave mode of interest are displayed as shown in Fig. 4. The results presented in Fig. 8 show how the technique is able to detect wave packets present in the

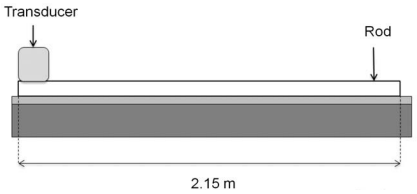

Fig. 9. Experimental setup diagram for an aluminum rod of 8-mm diameter; the transducer employed corresponds to a piezoelectric transducer [23].

signal, discriminating the specific wave mode for each of them and eliminating the effect of the dispersion. This is solved in a multimode scenario without any need for a predefined distance range and no previous information about the location of the different echoes and to which mode they correspond, as opposed to previous approaches [15], [17].

IV. Experimental Analysis

A. Experimental Procedure

The performance of both PuC and dispersion compensation techniques using the previous three excitation waveforms (Hann-windowed tone burst, the chirp and the Barker code) is now evaluated on an experimental case. An aluminum rod, as was conducted in the simulation presented in Section III, was employed with a pulse-echo configuration, described in Fig. 9. In order to replicate the same conditions of the simulated case, the analysis focused again on the first 2 ms of the response where three wave packets are present, L(0,1) first and second echoes and the F(1,1) first echo.

B. Results

Fig. 10 shows the performance of the three excitation waveforms (10-cycles Hann-windowed, Barker code 13-bit length sequence and chirp) after cross correlation with dispersion compensation of L(0,1) and F(1,1) for each specific length, 8.6 and 4.3 m, respectively.

The general performance of the method for the three waveforms is mainly poorer than the synthetic case. This is due to the simplifications made in the simulated case where the attenuation experienced by the waves and the transfer function of the transducers were not taken into account. In addition, any discrepancy between the theoretical dispersion curves and the real behavior would affect the performance of the method. This is especially clear for the Hann-windowed waveform [Fig. 10(a)] where a more severe superposition of both F(1,1) and L(0,1) echoes compared with the simulated case (Fig. 6) is shown. The superposed waveforms appear as a single wave packet, which makes the signal interpretation unmanageable. Therefore, the quantification of the SNR, resolution and ToA values is not applicable for these signals. The performance of both Barker code and chirp excitation proved to improve the temporal-spatial resolution of both echoes providing accurate information about the ToA. Resolution values, SNR and ToA accuracy were quantified and are included in Table IV. Resolution values, as in the synthetic case, show a better performance of chirp compared with Barker code, especially for the F(1,1) echo. The SNR is also higher for chirp excitation waveform for both echoes, F(1,1) and L(0,1). Finally, for the

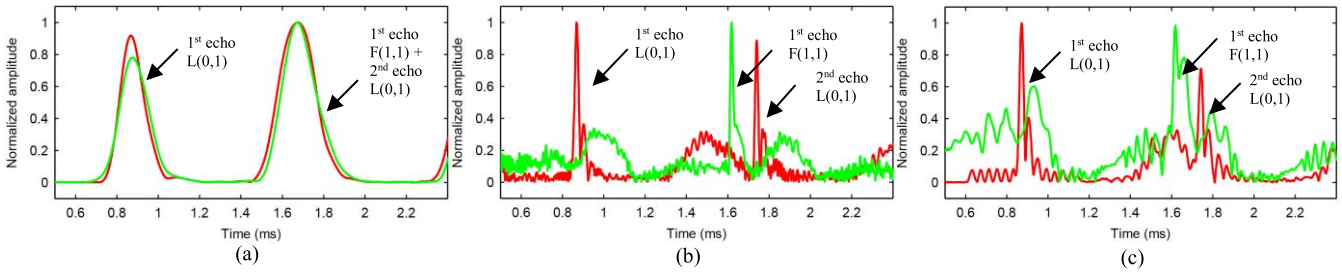

Fig. 10. Experimental results from an aluminum bar for (a) Hann-windowed, (b) Barker code, and (c) chirp excitation waveforms. Red and green lines represent the cross-correlated signal after dispersion compensation for L(0,1) and F(1,1) wave modes.

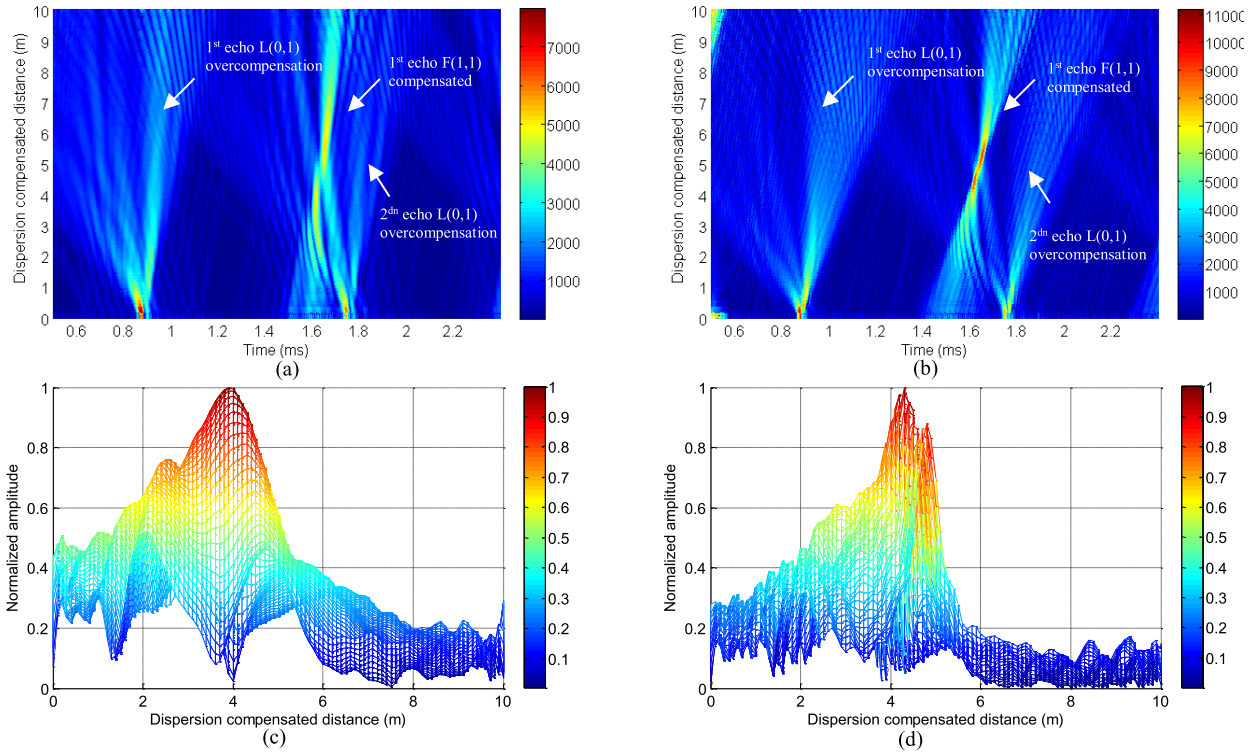

Fig. 11. Two-dimensional compressed diagram of the experimental results for F(1,1) dispersion compensation for (a) Barker code and (b) chirp excitation waveforms, for a dispersion compensated distance range of [0–10 m]. Dispersion compensated distances axis representation of the previous 2-D compressed diagrams focused on the time range of the reconstruction of F(1,1) echo for (c) Barker code and (d) and chirp excitation waveforms.

TABLE IV
EXPERIMENTAL RESULTS

Waveform	Wave mode	SNR (dB)	Resolution (μs)	ToA error (%)
Barker code	L(0,1)	13.44	30	3.15
	F(1,1)	12.84	49	3.35
Chirp	L(0,1)	16.88	22	2.91
	F(1,1)	19.93	48	3.35

ToA accuracy, both waveforms (Barker code and chirp) present similar results with minimum errors in both cases. For the ToA and resolution, both experimental and simulated results confirm the potential of this method.

Regarding the dispersion compensation performance, the method is able to successfully discriminate both wave modes F(1,1) and L(0,1). In order to study the cross-correlation response over a range of dispersion compensated signals, a 2-D compressed diagram was used, as in Section III. Fig. 11(a) and (b) shows how the dispersion compensation of chirp and Barker code is able to reshape F(1,1) echo for a dispersion compensated distance value of 4.3 m. The same procedure generates distortion due to overcompensation on both L(0,1) echoes, affecting the amplitude of their cross correlation response. As can be observed in Fig. 11 (a) and (b) for the chirp excitation, the technique is able to reconstruct the F(1,1) echo with higher amplitude and resolution than the Barker code case. These results agree with the previous SNR and resolution analysis. As discussed in Section III, the information provided by these 2-D diagrams can be used as a ToA calculation technique. In order to illustrate this, the F(1,1) echo is presented for the dispersion compensated distance domain [Fig. 11(c) and (d)].

C. APD Algorithm Performance Analysis for Experimental Signals

The APD algorithm is now applied to the experimental data. Fig. 12, top and bottom, shows the results for both the Barker code and the chirp, respectively. In both cases,

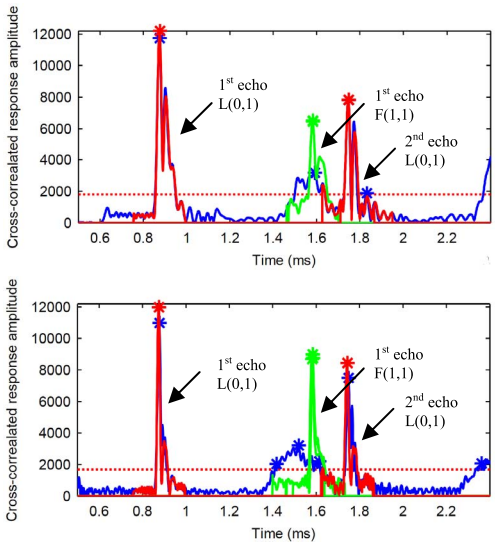

Fig. 12. Iterations' representation of algorithm result for the Barker code (top) and the chirp (bottom) excitation. Blue lines: first cross correlation result. Green lines: flexural compensated iterative results after cross correlation. Red lines: longitudinal compensated iterative results after cross correlation.

the iterative algorithm is able to detect the three wave packets present in the signal, two longitudinal echoes (red) and a flexural echo (green). Regarding the points of interest studied by the algorithm as possible echoes, a small number was again selected for simplification. These results, as in the simulated case (Fig. 8) show how the technique is able to detect both dispersive and nondispersive wave packets, discriminating the specific wave mode for each of them.

V. Conclusion

This paper presented a 2-D compressed analysis which combines both PuC and dispersion compensation techniques in order to improve the SNR, temporal-spatial resolution and extract accurate ToA of UGW responses.

The performance of the two proposed excitation waveforms, the Barker code and chirp, was compared with the traditionally used Hann-widowed tone burst. The results, both simulated and experimental, demonstrated the enhancement of ToA and temporal-spatial resolution for these two alternative waveforms. The combination of both techniques also proved to be a powerful tool for mode discrimination for both synthetic and experimental signals for Barker code and chirp waveforms. In contrast, Hann-windowed waveforms failed to discriminate the wave modes of concern.

As illustrated with 2-D compressed diagrams, the correct dispersion compensation is able to reconstruct the dispersive waves. In addition, the effect of the compensation of other wave modes present in the signal was studied and considered as opposed to traditional approaches [17]. The results show how, thanks to the overcompensation of these waves, the amplitude of their cross correlation response is highly reduced. The 2-D compressed diagrams show how the technique successfully recovers the F(1,1) echo and attenuates both L(0,1) echoes for both Barker code and chirp waveforms. These results have shown the superior performance of chirp compared with Barker code waveform regarding spatial resolution, SNR, and ToA extraction accuracy and also for wave mode discrimination purposes. The authors attribute this behavior to the better MLW and SLL values of chirp in comparison with Barker code.

The 2-D compressed analysis has been shown to be effective in recovering the dispersive waves, but the specific value for the compensation is required. For its *in situ* applications, the manual intervention is removed with an iterative APD algorithm, which evaluates different points of the signal separately. If a candidate point recovers the wave packet after dispersion compensation, the correct dispersion compensation is applied and therefore corresponds to an echo of the wave mode of interest. The proposed APD algorithm has been tested with both synthetic and experimental data for chirp and Barker code waveforms. The results have proved how the algorithm is able to discriminate the wave packets present in the signal as well as to which mode they correspond. A threshold and range of study for each candidate echo is selected to complete the automatization process. The level of the threshold will determine the candidate points and therefore must be set according to the sensitivity required by the system. This paper has focused on an area of the dispersion curves where both F(1,1) and L(0,1) present large differences in the dispersion behavior. Further analyses are required to study the applicability of the technique under different dispersive scenarios as well as its dependence on the correct dispersion curves. The authors also recommend further analysis under different noise levels as well as additional wave modes.

References

[1] J. L. Rose, *Ultrasonic Guided Waves in Solid Media*. Cambridge, U.K.: Cambridge Univ. Press, 2014.
[2] P. D. Wilcox, M. Lowe, and P. Cawley, "The effect of dispersion on long-range inspection using ultrasonic guided waves," *NDT E Int.*, vol. 34, no. 1, pp. 1–9, 2001.
[3] P. D. Wilcox, "A rapid signal processing technique to remove the effect of dispersion from guided wave signals," *IEEE Trans. Ultrason., Ferroelect., Freq. Control*, vol. 50, no. 4, pp. 419–427, Apr. 2003.
[4] R. Sicard, J. Goyette, and D. Zellouf, "A numerical dispersion compensation technique for time recompression of Lamb wave signals," *Ultrasonics*, vol. 40, nos. 1–8, pp. 727–732, 2002.
[5] L. De Marchi, A. Marzani, and M. Miniaci, "A dispersion compensation procedure to extend pulse-echo defects location to irregular waveguides," *NDT E Int.*, vol. 54, pp. 115–122, Mar. 2013.
[6] T. N. Tran, K.-C. T. Nguyen, M. D. Sacchi, and L. H. Le, "Imaging ultrasonic dispersive guided wave energy in long bones using linear radon transform," *Ultrasound Med. Biol.*, vol. 40, no. 11, pp. 2715–2727, 2014.
[7] T. N. Tran, L. H. Le, M. D. Sacchi, V.-H. Nguyen, and E. H. Lou, "Multichannel filtering and reconstruction of ultrasonic guided wave fields using time intercept-slowness transform," *J. Acoust. Soc. Amer.*, vol. 136, no. 1, pp. 248–259, 2014.
[8] K. Xu, D. Ta, P. Moilanen, and W. Wang, "Mode separation of Lamb waves based on dispersion compensation method," *J. Acoust. Soc. Amer.*, vol. 131, no. 4, pp. 2714–2722, 2012.
[9] K. Xu, D. Ta, B. Hu, P. Laugier, and W. Wang, "Wideband dispersion reversal of Lamb waves," *IEEE Trans. Ultrason., Ferroelect., Freq. Control*, vol. 61, no. 6, pp. 997–1005, Jun. 2014.
[10] T. H. Gan, D. A. Hutchins, D. R. Billson, and D. W. Schindel, "The use of broadband acoustic transducers and pulse-compression techniques for air-coupled ultrasonic imaging.," *Ultrasonics*, vol. 39, no. 3, pp. 94–181, 2001.
[11] T. H. Gan, D. A. Hutchins, R. J. Green, M. K. Andrews, and P. D. Harris, "Noncontact, high-resolution ultrasonic imaging of wood samples using coded chirp waveforms," *IEEE Trans. Ultrason., Ferroelectr., Freq. Control*, vol. 52, no. 2, pp. 280–288, Feb. 2005.

[12] M. Garcia-Rodriguez, Y. Yañez, M. J. Garcia-Hernandez, J. Salazar, A. Turo, and J. A. Chavez, "Application of Golay codes to improve the dynamic range in ultrasonic Lamb waves air-coupled systems," *NDT E Int.*, vol. 43, no. 8, pp. 677–686, 2010.
[13] Z. Zhou *et al.*, "Application of wavelet filtering and Barker-coded pulse compression hybrid method to air-coupled ultrasonic testing," *Nondestruct. Test. Eval.*, vol. 29, no. 4, pp. 297–314, 2014.
[14] Z. Luo, J. Lin, L. Zeng, and F. Gao, "Mode purification for ultrasonic guided waves under pseudopulse excitation," *J. Phys., Conf. Ser.*, vol. 628, no. 1, p. 012123, 2015.
[15] J. Lin, J. Hua, L. Zeng, and Z. Luo, "Excitation waveform design for Lamb wave pulse compression," *IEEE Trans. Ultrason., Ferroelectr., Freq. Control*, vol. 63, no. 1, pp. 165–177, Jan. 2016.
[16] M. K. Yücel *et al.*, "Pulse-compression based iterative time-of-flight extraction of dispersed ultrasonic guided waves," in *Proc. IEEE 13th Int. Conf. Ind. Inf. (INDIN)*, Jul. 2015, pp. 809–815.
[17] M. K. Yücel *et al.*, "Coded waveform excitation for high-resolution ultrasonic guided wave response," *IEEE Trans. Ind. Inf.*, vol. 12, no. 1, pp. 257–266, Jan. 2016.
[18] M. G. M. Hussain, "Principles of high-resolution radar based on nonsinusoidal waves. I. Signal representation and pulse compression," *IEEE Trans. Electromagn. Compat.*, vol. 31, no. 4, pp. 359–368, Nov. 1989.
[19] R. Y. Chiao and X. Hao, "Coded excitation for diagnostic ultrasound: A system developer's perspective," *IEEE Trans. Ultrason., Ferroelectr., Freq. Control*, vol. 52, no. 2, pp. 70–160, Feb. 2005.
[20] M. Legg, M. K. Yücel, V. Kappatos, C. Selcuk, and T.-H. Gan, "Increased range of ultrasonic guided wave testing of overhead transmission line cables using dispersion compensation," *Ultrasonics*, vol. 62, pp. 35–45, Sep. 2015.
[21] H. Zhao, L. Y. L. Mo, and S. Gao, "Barker-coded ultrasound color flow imaging: Theoretical and practical design considerations," *IEEE Trans. Ultrason., Ferroelectr., Freq. Control*, vol. 54, no. 2, pp. 319–331, Feb. 2007.
[22] M. Pollakowski and H. Ermert, "Chirp signal matching and signal power optimization in pulse-echo mode ultrasonic nondestructive testing," *IEEE Trans. Ultrason., Ferroelectr., Freq. Control*, vol. 41, no. 5, pp. 655–659, Sep. 1994.
[23] S. Fateri, P. S. Lowe, B. Engineer, and N. V. Boulgouris, "Investigation of ultrasonic guided waves interacting with piezoelectric transducers," *IEEE Sensors J.*, vol. 15, no. 8, pp. 4319–4328, Aug. 2015.

Sergio Malo received the M.Eng. degree in industrial engineering from the University of Castilla-La Mancha, Ciudad Real, Spain, in 2014. He is currently pursuing the Ph.D. degree in mechanical, aerospace, and civil engineering with Brunel University London, Uxbridge, U.K.

Since 2014, he has been with Brunel University London, where he was a Project Technical Assistant. In 2017, he joined the Smart Nondestructive Testing Group, Brunel Innovation Center, Brunel University London, where he is currently a Research Assistant. His research interests include signal processing of ultrasonic guided waves (UGW) applied to complex structures, the development of novel UGW applications, coded excitation waveforms, signal processing, and condition monitoring.

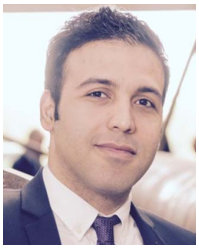

Sina Fateri received the B.Sc. (Hons.) degree in computer science from the University of Mazandaran, Babolsar, Iran, in 2009, and the M.Sc. (Distinction) degree in wireless communications engineering from Brunel University London, Uxbridge, U.K., in 2011. He completed the Ph.D. degree in electronic systems research based at TWI Ltd., Cambridge, U.K. in November 2015.

He was a Teaching Assistant with the Wireless Communications Laboratory at Brunel University London, from 2011 to 2013. Since 2015, he has been a Project Leader with Plant Integrity Ltd., Cambridge, where he is involved in performing signal processing for industrial sectors. He is the leader of the signal processing roadmap in Plant Integrity and his research interests include acoustic signal processing, wave mode identification, ultrasonic guided wave mode conversion from discontinuities, statistical methods, and long-term monitoring of large complex structures.

Dr. Fateri was given the title of Charted Engineer from The Welding Institute in 2017.

Makis Livadas received the bachelor's and master's degrees in electronics engineering from the University of Bucharest, Bucureşti, Romania. He received the Ph.D. degree from Imperial College London, London, U.K., with a focus on the subject of digital signal processing algorithms applied to imaging interpolation.

He has contributed to the software development of a variety of commercially available products. Most recently he has developed the Firmware for Plant Integrity Tele Focus which is a very successful product used for long-range guided wave ultrasonic testing. His current research interests include how to deploy software technology and signal processing algorithms to solve NDT problems and how to deliver these solutions to the end user of NDT technology.

Cristinel Mares received the M.Eng. degree in aerospace engineering and the Ph.D. degree in the development of methods for dynamic model updating for complex vibrating structures from the Politehnica University of Bucharest, Bucureşti, Romania.

He was with the Politecnico di Torino, Torino, Italy, and the University of Liverpool, Liverpool, U.K. He is currently a Senior Lecturer in Aerospace Engineering with Brunel University London, Uxbridge, U.K. He has authored over 100 papers in journals and refereed conferences. His current research interests include the development of techniques for structural health monitoring using vibration analysis, acoustic emission, and ultrasonic guided waves.

Dr. Mares is a Charted Engineer and fellow of the Institute of Mechanical Engineers and a member of the Institute of Physics, U.K.

Tat-Hean Gan received the bachelor's degree (Hons.) in electrical and electronics engineering from the University of Nottingham, Nottingham, U.K., the M.Sc. degree (with a distinction) in advanced mechanical engineering from the University of Warwick, Coventry, U.K., in 1998, and the Executive M.B.A. degree from the University of Birmingham, Birmingham, U.K. He is currently pursuing the Ph.D. degree in engineering with the University of Warwick, with a focus on advanced ultrasonic imaging.

He has worked as an academic and in industry for many years. He is currently a Professor with Brunel University London, London, U.K., where he is also the Chair of Acoustic Waves Technologies with the School of Engineering and Design. He has published more than 100 papers and has contributed to several books in the field of nondestructive testing. His current research interests include signal and image processing, sensor development, asset integrity management, and structural assessment.

Dr. Gan was a recipient of The Welding Institute Lidstone Award who is deemed to have made the most significant contribution to the advancement of welding technology. He was a recipient of CEng, EurIng, and IntPE(U.K.) status and has been a fellow of the Institute of Engineering and Technology and the British Institute of Nondestructive Testing, since 2011. He is also an Associate Director with TWI Ltd., and Technology Director with the National Structural Integrity Research Center, the U.K.'s first industry-led postgraduate education and research center in structural integrity.